International Journal of Scientific Research in Science and Technology
Print ISSN: 2395-6011 | Online ISSN: 2395-602X (www.ijsrst.com)
doi : https://doi.org/10.32628/IJSRST

Design and Analysis of a Novel Fuzzy Logic Controller Based AFLL Topology for Grid Connected PV System

Thalla Bharathi[1] , Dr. I. Prabhakar Reddy[2]

[1]M.Tech student, Dept of EEE, N B K R Institute of Science and Technology, Vidyanagar, Andhra Pradesh , India

[2]Professor, Dept of EEE ,N B K R Institute of Science and Technology, Vidyanagar, Andhra Pradesh, India

Article Info
Volume 9, Issue 6
Page Number : 547-557

Publication Issue
November-December-2022

Article History
Accepted : 05 Dec 2022
Published : 20 Dec 2022

ABSTRACT

This research provides an advanced frequency locked loop (AFLL) architecture for grid-connected PV systems that is based on fuzzy logic control (FLC). The FLC's interlinking with AFLL offers grid-connected PV systems both advantages. One artificial intelligence technology that offers fast reaction to system disruptions is the FLC. The proposed grid-connected PV system's performance is enhanced by the FLC-AFLL control architecture across a variety of disturbances, including polluted grid conditions, fault conditions, and load shifts. This suggested design would lessen harmonics in grid-connected PV systems and decrease load current disturbance. By injecting/absorbing active and reactive energy into grid-connected PV systems, FLC-AFLL control architecture enhances power quality in a long-distance radial transmission system. The entire proposed system performance is tested by using MATLAB/SIMULINK software.

Keywords : Advanced frequency locked loop (AFLL), maximum power point tracking (MPPT), power quality (PQ), photovoltaic (PV), voltage source converter (VSC).

I. INTRODUCTION

In the present, renewable energy systems (RES) Solar photovoltaic (PV), biogas, wind, and hydro energy systems are gaining popularity as an alternative to traditional energy sources for producing power. Because of its minimal maintenance and abundant supply of PV energy, it emerges as the ideal alternative to traditional energy. However, the grid in India is quite inadequate and damaged. Power quality (PQ) issues in the grid cause equipment linked to the distribution network to malfunction. The local load linked to the network is nonlinear, which is the root cause of the PQ issue [1]–[4]. The PQ problem's grid level is determined by PQ indices [5]. [6] Provides examples of several techniques for improving the local load linked to the network is nonlinear, which is the root cause of the PQ issue [1]–[4]. The PQ problem's grid level is determined by PQ indices [5]. The PQ of the grid may be improved using a variety of

techniques, as shown in [6]. A voltage source converter is used to lessen the PQ issues (VSC).

According to [7], this VSC functions as a distribution static compensator (DSTATCOM). The PV array can feed electricity to the grid and the load network at a unity power factor with the help of this VSC (UPF). [8] Presents a technique for modelling and simulating PV arrays. PV system productivity is based on power extraction using maximum power point tracking (MPPT). The several MPPT controls are detailed in [9] in various ways. The MPPT approach based on perturb and observe (P&O) is provided in [10], [11].

In the literature, many control methods for VSC have been demonstrated. Synchronous reference frame theory has been given by Kanjiya et al. [12] for controlling dynamic voltage restorers. The steady state performance of this method is good. However, a double frequency component is produced in the in-phase component, which reduces the performance of the system under load perturbation and other disturbances. For the purposes of balancing grid currents, controlling the point of common interaction (PCI) voltage, operating UPFs, and compensating for reactive power, a PQ theory-based instantaneous reactive power theory-based control for VSC is described in [13]. The least mean fourth (LMF), normalised least mean square (LMS), multistage least mean square (LMS), and other methods are compared in [14]. [15] Describes an adaptive Lorentzian norm-based filter for an isolated system. [16] Describes another adaptive filter for recursive least squares load voltage correction for battery-powered systems. The convergence rate has an impact on the performance of the adaptive filters during system dynamics, making them sensitive to changes in the system parameter. As a result, improving the system responsiveness under various dynamic settings requires the creation of control algorithms. [17] Presents a grid interfaced RES with a higher order passive filter based on an L (LCL) 2 filter.[18] shows a different hybrid filter that uses a passive filter and an active shunt filter using conservative power theory. When there is a dc offset in the load currents, the system behaviour under the aforementioned settings degrades. Generalized integrator (GI)-based controls are used to reduce the dc component's exposure to currents. In [19], a second order-based GI (SOGI) is described for the grid's UPF operation. The SOGI-PLL algorithm has been refined, and Xie et al. [20] have examined various techniques for rejecting dc offset for a single phase system. [21] Describes a dual SOGI-based control. [22] Describes a different approach to phase compensation using low order GI.

The ineffective rejection of higher order harmonics causes the responsiveness of these GI-based controls to decrease. In [23], a suggested adaptive vectorial filter-based control was created. A sophisticated frequency adaption loop has been incorporated in this control.

For the extraction of the fundamental component of the load current (FCLC) under challenging conditions such as harmonics distortion, solar insolation variation, load unbalancing, dc offset, and voltage swell/ sag, an advanced frequency locked loop (AFLL) algorithm with a greatly simplified FLL is reported in [24].

The remaining paper is organised as follows. The system description is described in section II, proposed system of the project is described in section III, results and discussion is described in section IV, conclusion and references are described in section V and VI.

II. SYSTEM DESCRIPTION

Figure 1 depicts the design of an LCL-filtered grid-connected inverter linked to a weak grid. VDC stands for R1, R2, L1, and L2 indicate the filter resistance and inductance values, Cf represents the filter capacitance, and Lg represents the grid inductance induced by the weak grid. There are just two grid-side currents and the DC-link. voltage are measured by the

suggested grid voltage sensorless current control approach in Fig. 1. In Fig. 1, the inverter system may be stated mathematically as follows when grid impedance is absent:

$$pi_2^q = (-R_2/L_2)i_2^q - \omega i_2^d + (1/L_2)v_c^q - (1/L_2)e^q \quad (1)$$

$$pi_2^d = (-R_2/L_2)i_2^d + \omega i_2^q + (1/L_2)v_c^d - (1/L_2)e^d \quad (2)$$

$$pi_1^q = (-R_1/L_1)i_1^q - \omega i_1^d - (1/L_1)v_c^q + (1/L_1)v_i^q \quad (3)$$

$$pi_1^d = (-R_1/L_1)i_1^d + \omega i_1^q - (1/L_1)v_c^d + (1/L_1)v_i^d \quad (4)$$

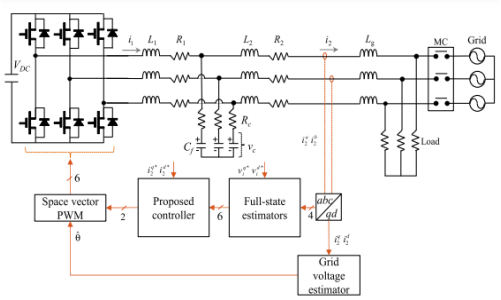

FIGURE 1. Configuration of a grid-connected inverter and a current control scheme.

$$pv_c^q = -\omega v_c^d - (1/C_f)i_2^q + (1/C_f)i_1^q \quad (5)$$

$$pv_c^d = \omega v_c^q - (1/C_f)i_2^d + (1/C_f)i_1^d \quad (6)$$

I1 is the inverter-side current, i2 is the grid-side current, Vc is the capacitor voltage, e is the grid voltage, vi is the inverter output voltage, and is the angular frequency of the grid voltages. Where the superscripts "q" and "d" signify the q-axis and d-axis variables, respectively. The state-space model of the inverter system is represented as from (1) to (6).

$$\dot{\mathbf{x}}(t) = \mathbf{A}\mathbf{x}(t) + \mathbf{B}\mathbf{u}(t) + \mathbf{D}\mathbf{e}(k) \quad (7)$$

$$\mathbf{y}(t) = \mathbf{C}\mathbf{x}(t) \quad (8)$$

In this case, $x = I_q{}^2\ I_d{}^2\ I_q{}^1\ I_d{}^1\ v^{q}{}_c\ v^{d}{}_c]$ $u = [v^{q}{}_I\ v^{d}{}_I]^T$ is the system state vector. $e = [e_q\ e_d]^T$ is the system's input vector. The system matrices A, B, C, and D are represented as (9), which is given at the bottom of the page. T is the grid voltage vector. The zero-order hold (ZOH) approach with sample time Ts is used to produce a discretized model of the continuous-time inverter system described by (7) and (8) for the purpose of a digital implementation, as shown below:

$$\mathbf{A} = \begin{bmatrix} -R_2/L_2 & -\omega & 0 & 0 & 1/L_2 & 0 \\ \omega & -R_2/L_2 & 0 & 0 & 0 & 1/L_2 \\ 0 & 0 & -R_1/L_1 & -\omega & -1/L_1 & 0 \\ 0 & 0 & \omega & -R_1/L_1 & 0 & -1/L_1 \\ -1/C_f & 0 & 1/C_f & 0 & 0 & -\omega \\ 0 & -1/C_f & 0 & 1/C_f & \omega & 0 \end{bmatrix}$$

$$\mathbf{B} = \begin{bmatrix} 0 & 0 \\ 0 & 0 \\ 1/L_1 & 0 \\ 0 & 1/L_1 \\ 0 & 0 \\ 0 & 0 \end{bmatrix}, \quad \mathbf{D} = \begin{bmatrix} 1/L_2 & 0 \\ 0 & 1/L_2 \\ 0 & 0 \\ 0 & 0 \\ 0 & 0 \\ 0 & 0 \end{bmatrix}$$

$$\mathbf{C} = \begin{bmatrix} 1 & 0 & 0 & 0 & 0 & 0 \\ 0 & 1 & 0 & 0 & 0 & 0 \end{bmatrix} \quad (9)$$

$$\mathbf{x}(k+1) = \mathbf{A}_d\mathbf{x}(k) + \mathbf{B}_d\mathbf{u}(k) + \mathbf{D}_d\mathbf{e}(k) \quad (10)$$

$$\mathbf{y}(k) = \mathbf{C}_d\mathbf{x}(k) \quad (11)$$

where $\mathbf{A}_d = e^{\mathbf{A}T_s}$, $\mathbf{B}_d = (\int_0^{T_s} e^{\mathbf{A}T_s}dt)\mathbf{B}$, $\mathbf{D}_d = (\int_0^{T_s} e^{\mathbf{A}T_s}dt)\mathbf{D}$ $\mathbf{C}_d = \mathbf{C}$.

III. GRID VOLTAGE SENSORLESS CURRENT CONTROLLER WITH ACTIVE DAMPING

A. INTEGRAL STATE FEEDBACK CONTROL WITH RESONANT CONTROLLER

The integral terms are added to the inverter state model to form an integral state feedback controller, which ensures asymptotic reference tracking and disturbance rejection. The full system model may be put together as follows by including the integral action in (10) and (11), according to [23], [24]:

$$\begin{bmatrix} \mathbf{x}(k+1) \\ \mathbf{x}_i(k+1) \end{bmatrix} = \begin{bmatrix} \mathbf{A}_d & \mathbf{0}_{6\times2} \\ -\mathbf{B}_i\mathbf{C}_d & \mathbf{A}_i \end{bmatrix} \begin{bmatrix} \mathbf{x}(k) \\ \mathbf{x}_i(k) \end{bmatrix} + \begin{bmatrix} \mathbf{B}_d \\ \mathbf{0}_{2\times2} \end{bmatrix} \mathbf{u}(k) + \begin{bmatrix} \mathbf{D}_d \\ \mathbf{0}_{2\times2} \end{bmatrix} \mathbf{e}(k) + \begin{bmatrix} \mathbf{0}_{6\times2} \\ \mathbf{B}_i \end{bmatrix} \mathbf{r}(k) \quad (12)$$

$$\mathbf{y}_s(k) = \begin{bmatrix} \mathbf{C}_d & \mathbf{0}_{2\times2} \end{bmatrix} \begin{bmatrix} \mathbf{x}(k) \\ \mathbf{x}_i(k) \end{bmatrix} \quad (13)$$

Where

$$\mathbf{x}_i(k+1) = \mathbf{A}_i\mathbf{x}_i(k) + \mathbf{B}_i\boldsymbol{\varepsilon}(k)$$

$$\boldsymbol{\varepsilon} = [\varepsilon^q\ \varepsilon^d]^T = \mathbf{r} - \mathbf{C}_d\mathbf{x}, \quad \mathbf{A}_i = \begin{bmatrix} 1 & 0 \\ 0 & 1 \end{bmatrix},$$

$$\mathbf{B}_i = \begin{bmatrix} T_s & 0 \\ 0 & T_s \end{bmatrix}$$

Xi = $[x^{q}{}_i,\ x^{d}{}_i]$ T is the integral state vector, r = $[i^{q*}{}_2\ i^{d*}{}_2]$ T is the reference current vector, 0m×n is a zero matrix with appropriate dimensions, and "*" represents the reference quantities Integral state feedback control is built as follows for an enhanced system in (12) and (13).

$$\mathbf{u}(k) = \begin{bmatrix} \mathbf{K}_x & \mathbf{K}_i \end{bmatrix} \begin{bmatrix} \mathbf{x}(k) \\ \mathbf{x}_i(k) \end{bmatrix}$$
$$\mathbf{K}_i = \begin{bmatrix} K_{i1}^q & K_{i2}^q \\ K_{i1}^d & K_{i2}^d \end{bmatrix} \quad (14)$$

Where Kx Ki represents the sum of state feedback gains. The linear quadratic regulator (LQR) approach is used to systematically determine the full-state feedback control gain by minimising the discrete quadratic cost function. The literature has a thorough block diagram of the state feedback current controller enhanced with integral control terms [23].

The suggested approach also employs parallel resonant controllers to track the grid-side current reference and to make up for grid voltage disruptions in the fifth- and seventh-order harmonic components. Using the transfer function provided as, the resonant control technique is implemented in the discrete-time domain.

$$G_{h=5,7}(z) = \frac{z^2 - \cos(h\omega T_s)z}{z^2 - 2\cos(h\omega T_s)z + 1}. \quad (15)$$

B. VOLTAGE SENSORLESS CURRENT CONTROL

The phase angles and frequency of three-phase grid voltages may be accurately estimated using a current-controller-based sensorless approach, which is shown in this section. To determine the grid phase angles and modify the phase angle between the grid voltage and grid-injected current, the conventional phase-locked loop approach is utilised. But instead of using grid voltage measurements to control the AC line currents as in the prior work [35], this research derives the grid phase angles from the integral term of d-axis current. The grid frequency is also calculated to implement the resonant controllers in (15). The grid phase angle and grid frequency estimator is made with this end in mind.

An LCL-filtered grid linked inverter system is changed to the reference frame that rotates with the estimated grid phase angle when the precise grid phase angle is unknown. The state equation in the SRF is created by discretizing the continuous-time inverter model (10). On the other hand, the inverter model in (10) is changed to when the continuous-time model at the rotating reference frame with is discretized.

$$\mathbf{x}(k+1) = \mathbf{A}_d\mathbf{x}(k) + \mathbf{B}_d\mathbf{u}(k) + \mathbf{D}_d\tilde{\mathbf{e}}(k) \quad (16)$$

Where

$$\tilde{\mathbf{e}} = [\tilde{e}_q \ \tilde{e}_d]^T = [e_q\cos(\tilde{\theta}) \ e_q\sin(\tilde{\theta})]^T$$

The above equation of grid voltage error vector caused by applying the transformation with an unknown grid phase angle, and $\tilde{\theta} = \theta - \hat{\theta}$ is the discrepancy between the real grid voltage phase angle θ and the estimated $\hat{\theta}$ value. It is clear that the representation of (16) is simplified to the LCL-filtered inverter model in the SRF as shown in once the difference reaches zero (10).

The d-axis current error is utilised as follows to estimate $\widetilde{e_d}$:

$$\frac{d}{dt}\hat{\tilde{e}}_d = \lambda(i_2^{d*} - i_2^d) \quad (17)$$

When the estimated values are denoted by "^" and the estimation gain is " $\widetilde{e_d}$, $\hat{\theta}$ "With the use of the estimation of e d, the following may be discovered under the assumption of $\tilde{\theta} \approx \sin\tilde{\theta}$ as follows

$$\tilde{\theta} \approx \sin(\tilde{\theta}) = \frac{\hat{\tilde{e}}_d}{e_q}. \quad (18)$$

The phase angle difference $\tilde{\theta}$is used to estimate the phase angle and frequency of the grid voltage by constructing the Luenberger observer based on the grid model as follows:

$$\frac{d}{dt}\theta = \omega \quad (19)$$
$$\frac{d}{dt}\omega = 0. \quad (20)$$

From the model in (19) and (20) with the phase angle difference $\tilde{\theta}$as an estimator input, the dynamic of the observer is constructed as follows:

$$\frac{d}{dt}\begin{bmatrix} \hat{\theta} \\ \hat{\omega} \end{bmatrix} = \begin{bmatrix} 0 & 1 \\ 0 & 0 \end{bmatrix}\begin{bmatrix} \hat{\theta} \\ \hat{\omega} \end{bmatrix} + \begin{bmatrix} \alpha \\ \beta \end{bmatrix}\tilde{\theta}. \quad (21)$$

Where α and β the observer gains are and. After a discretization procedure based on the Euler technique with the sample time T_s, the observer in (21) is implemented in the discrete-time domain. The observer poles are positioned inside the unit circle thanks to the design of the observer gains, α and β, and. Additionally, the estimated q-axis capacitor voltage is utilised instead of the estimated q-axis grid voltage magnitude owing to a low voltage loss via a small-size inductor because the suggested technique does not monitor the grid voltages for grid voltage sensorless operation [36]. As a result, the equation below is used to replace the grid phase error in equation (18).

$$\tilde{\theta} \approx \frac{\hat{\tilde{e}}_d}{e_q} \approx \frac{\hat{\tilde{e}}_d}{\hat{v}_c^q}. \quad (22)$$

C. ACTIVE DAMPING SCHEME

The state-feedback based AD approaches, which have the benefits of flexibility, robustness, and zero power loss, are favoured to repress the peak at resonance frequency from the LCL filter in order to assure the control stability of LCL-filtered grid connected inverters. However, a significant resonance frequency derivation is introduced by the presence of grid impedance or the changing of LCL filter settings. The state feedback current controller's capacity to suppress resonance and its control performance may suffer as a result.

An AD approach is included into the full-state feedback controller in this part to improve the system's stability and robustness against the detrimental effects of external perturbations like weak grid conditions or internal parameter uncertainty. When the intended resonance frequency and the actual resonance frequency are out of phase, resonance damping performance often suffers. The AD system should be designed to provide satisfactory performance over a wide range of resonance frequencies. In this section, an AD method is incorporated into the full-state feedback controller to increase the system's resilience and stability against harmful external perturbations like internal parameter uncertainty or poor grid conditions. Resonance dampening performance frequently worsens when the desired resonance frequency and the actual resonance frequency are out of phase. The AD scheme should be built in order to maintain acceptable performance throughout a broad range of resonance frequency.

The following is a presentation of the HPF transfer function for designing an extra AD scheme:

$$G_H(s) = \frac{y_h}{u_h} = 1 - \frac{\omega_c^2}{s^2 + 2\xi\omega_c s + \omega_c^2} \quad (23)$$

Where ξ the damping ratio is and the cut-off frequency is ωc. The aforementioned transfer function is represented as follows in the discrete-time state space to complement (23) with the system description in (12):

$$\mathbf{x}_h(k+1) = \mathbf{A}_h\mathbf{x}_h(k) + \mathbf{B}_h u_h(k) \quad (24)$$

$$y_h(k) = \mathbf{C}_h\mathbf{x}_h(k) \quad (25)$$

Where

$$\mathbf{A}_h = \begin{bmatrix} A_{h1} & A_{h2} \\ A_{h3} & A_{h4} \end{bmatrix}, \ \mathbf{B}_h = \begin{bmatrix} B_h \\ 0 \end{bmatrix}, \ \mathbf{C}_h = \begin{bmatrix} C_{h1} & C_{h2} \end{bmatrix}.$$

The integral control output u_i (k) in (14) is once again represented as in order to execute the AD scheme.

$$\mathbf{u}_i(k) = \mathbf{K}_i\mathbf{x}_i(k) = \begin{bmatrix} K_{i1}^q & K_{i2}^q \\ K_{i1}^d & K_{i2}^d \end{bmatrix} \begin{bmatrix} x_i^q \\ x_i^d \end{bmatrix} \quad (26)$$

Is used to modify the input in (24). Incorporating the signals from the integral control outputs of the q- and d-axes.

$$\mathbf{x}_H(k+1) = \mathbf{A}_H\mathbf{x}_H(k) + \mathbf{B}_H\mathbf{u}_i(k) \quad (27)$$

$$\mathbf{y}_H(k) = -\mathbf{C}_H\mathbf{x}_H(k) \quad (28)$$

Where xH = [x^{q}_{h1} x^{q}_{h2} x $^{d}_{h1}$ x^{d}_{h2}] T is the HPF state vector for the q-axis and d-axis, and the system matrices A_H, B_H, and C_H are expressed as follows:

$$\mathbf{A}_H = \begin{bmatrix} \mathbf{A}_h & 0 \\ 0 & \mathbf{A}_h \end{bmatrix}, \quad \mathbf{B}_H = \begin{bmatrix} B_h & 0 \\ 0 & 0 \\ 0 & B_h \\ 0 & 0 \end{bmatrix}$$

$$\mathbf{C}_H = \begin{bmatrix} C_{h1} & C_{h2} & 0 & 0 \\ 0 & 0 & C_{h1} & C_{h2} \end{bmatrix}.$$

The integral state equation in (12) and the HPF state equation in (27) are combined to create the following overall system model:

$$\begin{bmatrix} \mathbf{x}(k+1) \\ \mathbf{x}_i(k+1) \\ \mathbf{x}_H(k+1) \end{bmatrix} = \begin{bmatrix} \mathbf{A}_d & \mathbf{0}_{6\times2} & \mathbf{0}_{6\times4} \\ -\mathbf{B}_i\mathbf{C}_d & \mathbf{A}_i & \mathbf{0}_{2\times4} \\ \mathbf{0}_{4\times6} & -\mathbf{B}_{H1} & \mathbf{A}_H \end{bmatrix} \begin{bmatrix} \mathbf{x}(k) \\ \mathbf{x}_i(k) \\ \mathbf{x}_H(k) \end{bmatrix} + \begin{bmatrix} \mathbf{B}_d \\ \mathbf{0}_{2\times2} \\ \mathbf{0}_{4\times2} \end{bmatrix} \mathbf{u}(k) + \begin{bmatrix} \mathbf{D}_d \\ \mathbf{0}_{2\times2} \\ \mathbf{0}_{4\times2} \end{bmatrix} \mathbf{e}(k) + \begin{bmatrix} \mathbf{0}_{6\times2} \\ \mathbf{B}_i \\ \mathbf{0}_{4\times2} \end{bmatrix} \mathbf{r}(k)$$

$$\mathbf{B}_{H1} = \begin{bmatrix} K^q_{i1}B_h & K^q_{i2}B_h \\ 0 & 0 \\ K^d_{i1}B_h & K^d_{i2}B_h \\ 0 & 0 \end{bmatrix} \tag{29}$$

The state feedback control for the full system model in the suggested current control using the AD scheme results in (29). However, the proposed AD approach may lead to the issue of the HPFs' high frequency harmonic amplification. The amplitude of the anti-phase frequency is changed by increasing a factor of (0, 1, and 1) in the control law to resolve this issue. Section 4 will discuss the consequences of the AD based on the value of. The state feedback control term, integral state feedback control term, and AD term make up the whole control law from the augmented system in (29), as follows:

$$\mathbf{u}(k) = \begin{bmatrix} \mathbf{K}_x & \mathbf{K}_i & \zeta\mathbf{C}_H \end{bmatrix} \begin{bmatrix} \mathbf{x}(k) \\ \mathbf{x}_i(k) \\ \mathbf{x}_H(k) \end{bmatrix} \tag{30}$$

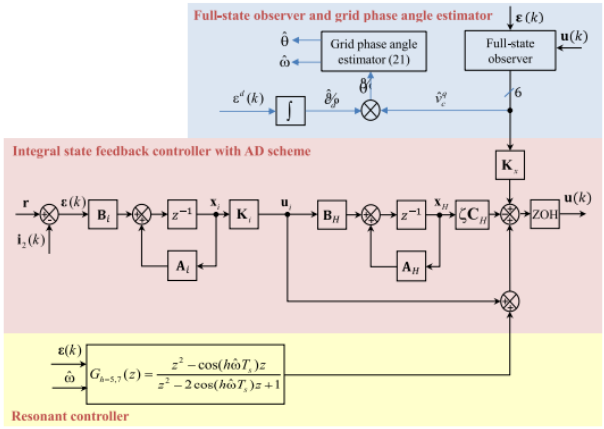

FIGURE 2. Detailed block diagram for the proposed grid voltage sensorless current control scheme with the grid phase angle estimator and AD scheme.

IV. Proposed method

Fuzzy logic controllers are used in a variety of renewable energy applications (FLC). Because of its ease of use, FLC has gained in popularity over the previous decade. FLC also handles bad input, removing the requirement for the controller to use a precise mathematical model. In order to acquire the greatest power from PV modules, FLC can simply manage nonlinearity problems. It can function in any weather, with any temperature or irradiance variation.

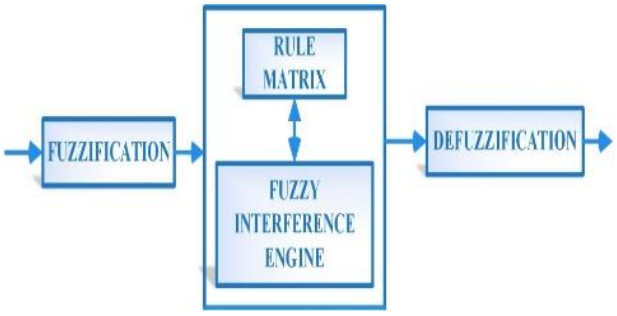

Fig.11. the Stages of Fuzzy Logic controller

There are three types of fuzzy logic controller processes:

1. Fuzzification
2. Rule Evaluation
3. Defuzzification

The first form of fuzzification allows crisp input, such as fluctuations in input voltage values. It uses the stored membership function to convert Crisp Input to Fuzzy Input. When the fuzzy values are designed, the first stage of FLC, fuzzification, occurs.

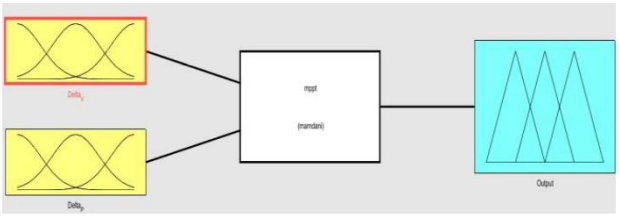

Fig.12. the FLC

The second type of Fuzzy logic controller is rule evaluation. During rule evaluation, the fuzzy processor is utilised to determine the controlling action that occurs during the response delivered to the set of input values. The Rule Evaluation gives a fuzzy output for each action. The last category in the fuzzy logic controller process is the Defuzzification Technique. The fuzzy value is turned to a crisp value during defuzzification. The crisp value from the fuzzy set is always the intended value of the output. Each fuzzy output variable in relation to the output membership function for each input set is effectively modified by the FLC Process. The centre of gravity (COG) methodology, often known as the centroid method, is the most commonly used defuzzification procedure. The Fuzzy logic controller is employed in the MPPT controller in this project, which is related to the P&O algorithm. FLC involvement in MPPT increases output voltage, and creating a Fuzzy Logic Controller that does not require much awareness of the model's specific requirements is relatively straightforward. The rule must only be assigned to each set of the membership function.

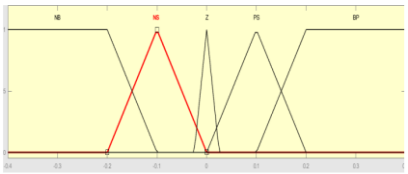

Fig.13. Membership function of input Variable Delta_P

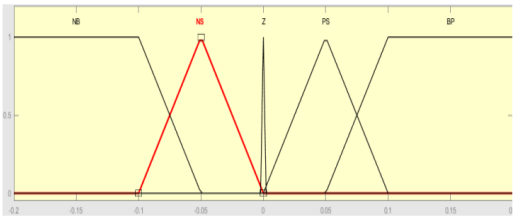

Fig.14. Membership function of input Variable Delta_V

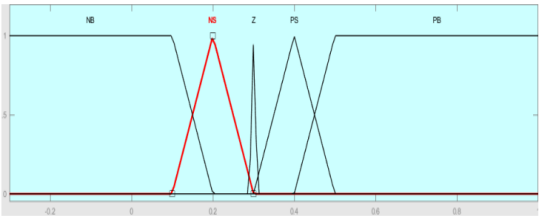

Fig.15. Membership function of Output Variable Delta_Y

ΔP / ΔV	NB	NS	Z	PS	PB
NB	PB	PS	NB	NS	NS
NS	PS	PS	NB	NS	NS
Z	NS	NS	NS	PB	PB
PS	NS	PB	PS	NB	PB
PB	NB	NB	PB	PS	PB

Table-1 Rule based in FLC

This paper introduces a novel method for constructing an MPPT for a PV module under unknown conditions. After implementing this method, the fluctuation around the Maximum PowerPoint is decreased. This technique outperforms the straightforward P&O algorithm Approach. Variations in PV module voltage (Delta V) and changes in PV module power are sent into the Fuzzy logic controller (Delta P). The fuzzy logic controller's output is delta Y. The fuzzy logic controller's output is delta Y. The output of the Fuzzy logic controller is fed into the sampling signal, which is altered and sent to the boost converter, which provides the switching pulses.

V. Simulation results:

The performance of the system is assessed by developing a model in MATLAB and testing it under a number of operating situations, including as load imbalance, uncertain solar insolation, and PCI voltage

fluctuation. Load currents (iLabc), PV array voltage (Vpv), grid currents (isabc), VSC currents (ivsc), PV array power (Ppv), grid active power (Ps), grid reactive power (Qs), terminal voltage amplitude (Vt), dc link voltage (Vdc), and solar insolation (G) are presented for various conditions. The appendices provide data from the system.

Simulation results using fuzzy logic controller:

Case_A

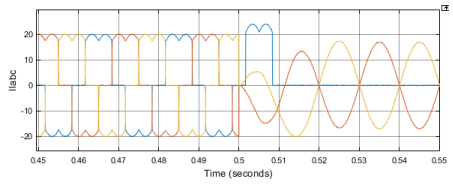

Ilabc

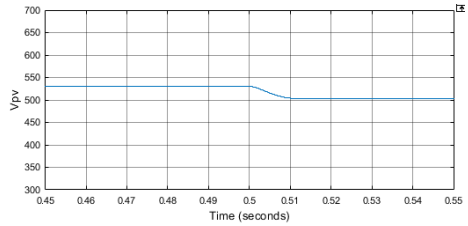

Vpv

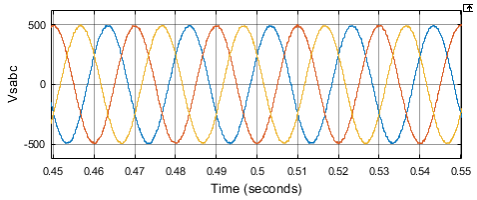

Vsabc

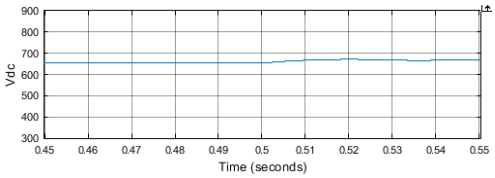

Vdc

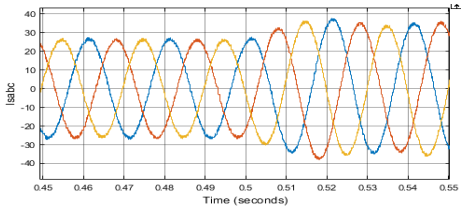

Isabc

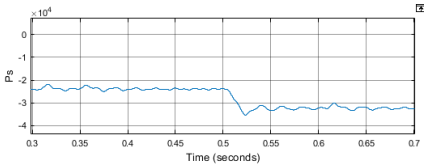

Ps

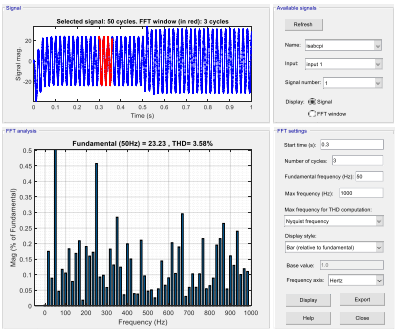

Using PI controller

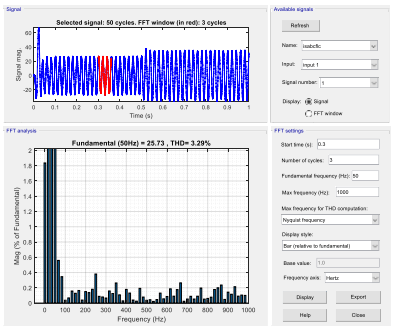

Using fuzzy logic controller

Case_b

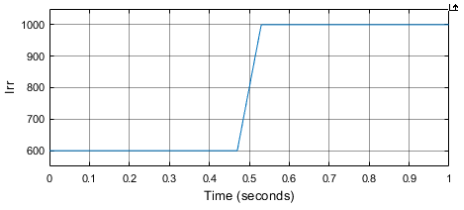

Irr

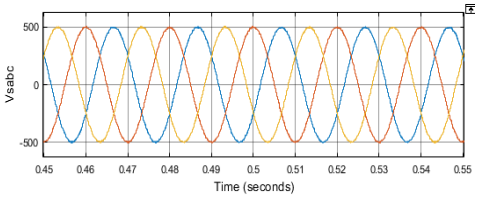

Vsabc

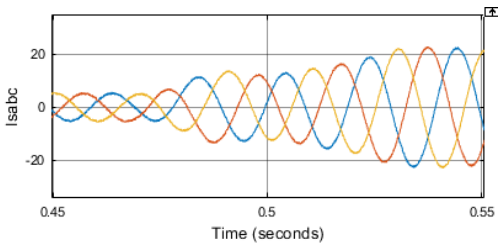

Isabc

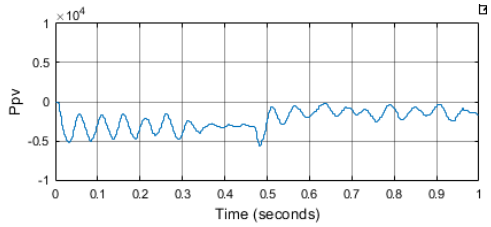

Ppv

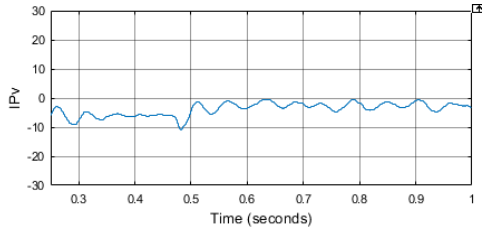

Ipv

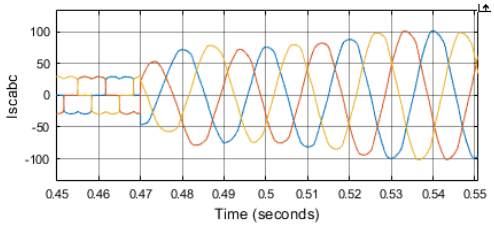

Iscabc

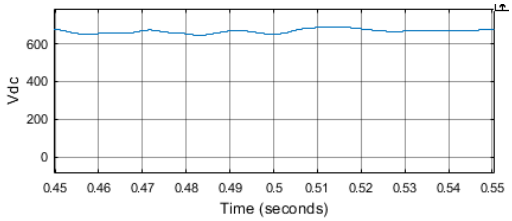

Vdc

Case_c

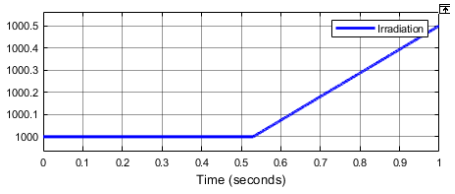

Irradiation

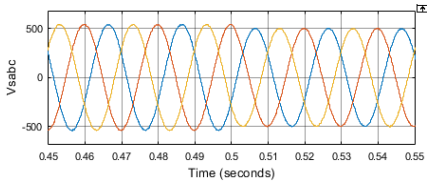

Vsabc

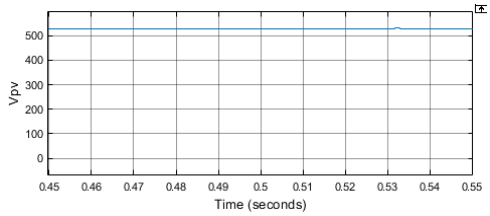

Vpv

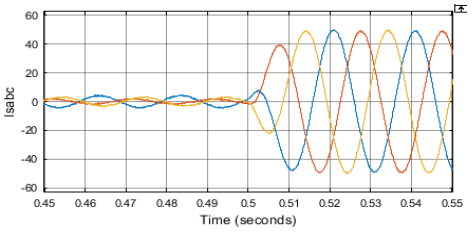

Isabc

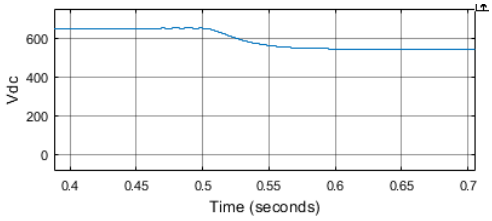

Vdc

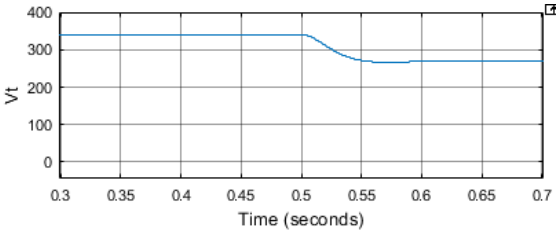

Vt

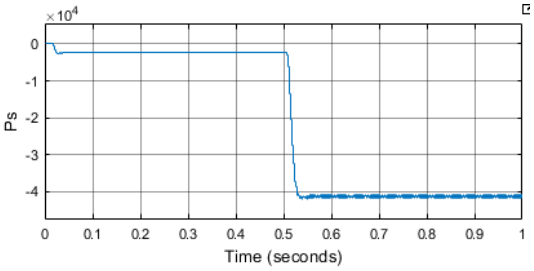

Ps

Case_e

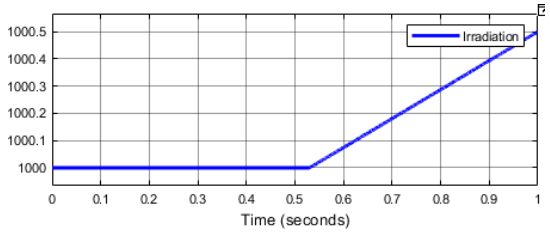

Irradiation

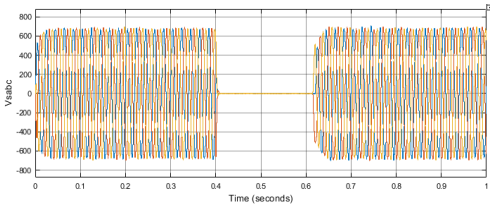

Vsabc

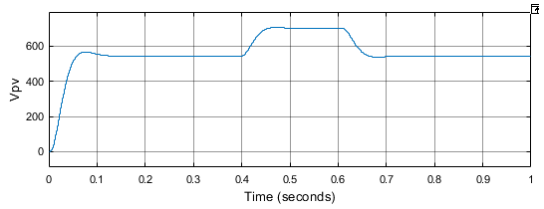

Vpv

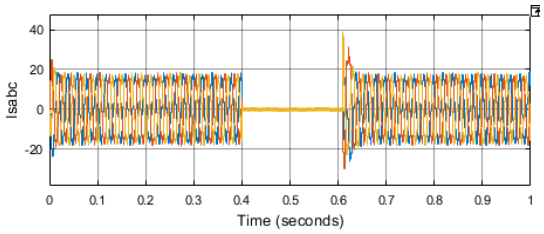

Isabc

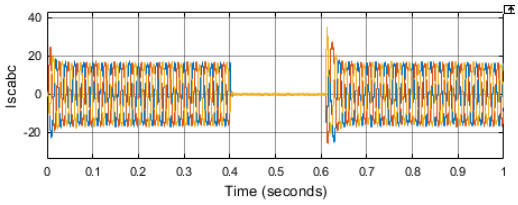

Iscabc

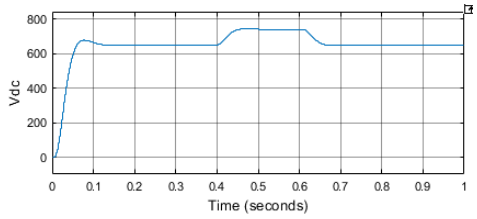

Vdc

5a

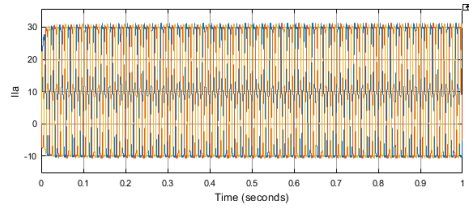

Ila

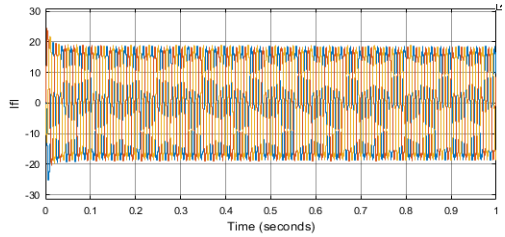

Ifl

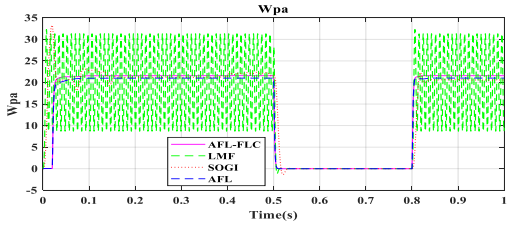

Comparative analysis of AFLL based fuzzy logic controller with conventional controls.

VI. Conclusion

In this paper concluded that the FLC-AFLL control topology provides best solution for Performance of a grid-connected PV system under various disturbances such as polluted grid, fault state, and load variations The FLC-AFLL performance compared to the proposed revolutionary FLC-AFLL design increases the performance of grid-connected PV systems in this study. The FLC-AFLL design minimises grid harmonics and load currents when compared to the FLL architecture. The simulation findings show which control structure is best for grid-connected PV systems under various shocks.

PARAMETER	AFL-PI CONTROLLER	AFL-FLC
Stator current	3.58	3.29

Thd comparison table Steady state performance of AFLL-FLC in comparison with other conventional control algorithms.

VII. REFERENCES

[1]. F. Blaabjerg, R. Teodorescu, M. Liserre, and A. V. Timbus, "Overview of control and grid synchronization for distributed power generation systems," IEEE Trans. Ind. Electron., vol. 53, no. 5, pp. 1398–1409, Oct. 2006.

[2]. B. Kroposki, B. Johnson, Y. Zhang, V. Gevorgian, P. Denholm, B.-M. Hodge, and B. Hannegan, "Achieving a 100% renewable grid: Operating electric power systems with extremely high levels of variable renewable energy," IEEE Power Energy Mag., vol. 15, no. 2, pp. 61–73, Mar. 2017.

[3]. I. Akhtar, S. Kirmani, and M. Jameel, "Reliability assessment of power system considering the impact of renewable energy sources integration into grid with advanced

intelligent strategies," IEEE Access, vol. 9, pp. 32485–32497, 2021.

[4]. Y. Han, M. Yang, H. Li, P. Yang, and F. Blaabjerg, "Modeling and stability analysis of LCL-type grid-connected inverters a comprehensive overview," IEEE Access, vol. 7, pp. 114975–115001, 2019.

[5]. R. N. Beres, X. Wang, M. Liserre, F. Blaabjerg, and C. L. Bak, "A review of passive power filters for three-phase grid-connected voltage-source converters," IEEE Trans. J. Emerg. Sel. Topics Power Electron., vol. 4, no. 1, pp. 54–69, Mar. 2016.

[6]. X. Wang, F. Blaabjerg, and P. C. Loh, "Design-oriented analysis of resonance damping and harmonic compensation for LCL-filtered voltage source converters," in Proc. IEEE Int. Power Electron. Conf., May 2014, pp. 216–223.

[7]. W. Wu, Y. Liu, Y. He, H. S.-H. Chung, M. Liserre, and F. Blaabjerg, "Damping methods for resonances caused by LCL-filter-based current controlled grid-tied power inverters: An overview," IEEE Trans. Ind. Electron., vol. 64, no. 9, pp. 7402–7413, Sep. 2017.

[8]. W. Yao, Y. Yang, X. Zhang, F. Blaabjerg, and P. C. Loh, "Design and analysis of robust active damping for LCL filters using digital notch filters," IEEE Trans. Power Electron., vol. 32, no. 3, pp. 2360–2375, Mar. 2017.

[9]. R. Peña-Alzola, M. Liserre, F. Blaabjerg, M. Ordonez, and T. Kerekes, "A self-commissioning notch filter for active damping in a three-phase LCL-filter-based grid-tie converter," IEEE Trans. Power Electron., vol. 29, no. 12, pp. 6754–6761, Dec. 2014.

[10]. J. Yuan, A. Al Durra, and E. El-Saadany, "Adaptive digital notch filter based on online grid impedance estimation for grid-tied LCL filter systems," Electr. Power Syst. Res., vol. 172, pp. 183–192, Jul. 2019.

Cite this article as :

Thalla Bharathi, Dr. I. Prabhakar Reddy, "Design and Analysis of a Novel Fuzzy Logic Controller Based AFLL Topology for Grid Connected PV System", International Journal of Scientific Research in Science and Technology (IJSRST), Online ISSN : 2395-602X, Print ISSN : 2395-6011, Volume 9 Issue 6, pp. 547-557, November-December 2022.

Journal URL : https://ijsrst.com/IJSRST229683